NANO LETTERS

2008
Vol. 8, No. 11
3605-3612

Modeling the Self-Assembly of Colloidal Nanorod Superlattices

Alexey V. Titov and Petr Král*

Department of Chemistry, University of Illinois at Chicago, Chicago, Illinois 60607

Received May 28, 2008; Revised Manuscript Received September 30, 2008

ABSTRACT

We model the self-assembly of superlattices of colloidal semiconducting nanorods horizontally and vertically oriented on material substrates. The models include van der Waals and Coulombic coupling between nanorods with intrinsic electric dipoles and their coupling to the substrates. We also investigate the effect of external electric fields on the self-assembly processes. Our theoretical predictions for stable self-assembled superlattices agree well with the available experimental data.

1. Introduction. In recent years, many types of nanoparticles[1,2] (NPs) have been prepared and intensively studied for their rich spectrum of applications.[3−5] Nanorods (NRs) with nearly cylindrical shapes have been also prepared.[6,7] Today's semiconducting NRs[8−10] have well-determined aspect ratios,[11,12] similarly to metal nanorods.[13,14] Typical CdSe/CdS NRs have the lengths of $L \approx 5-40$ nm and diameters of $D \approx 3-10$ nm. Similarly to NPs,[15−17] their surfaces can be passivated with various surfactants, such as trioctylphosphine oxide (TOPO).

The NRs can be incorporated into matrices, such as conductive polymers[18,19] and biological systems.[20,21] They can be also self-assembled into superlattices of different lattice types that are formed on material surfaces (substrates).[12,22] The orientation of NRs on the substrates is critical for most applications. Therefore, the knowledge of experimental conditions under which different lattice types can be observed is crucial. However, reproducible self-assembly of NRs in certain configurations can be a tricky task.[23−26]

1.1. Experimental Observations. In Table 1, we summarize typical experimental data obtained for self-assembled semiconducting CdSe/CdS NRs. We can see a large variation of the NR sizes, characterized by the length L, diameter D, dipole moments μ, and assembly patterns. Similarly as in liquid crystal,[27] partial orientational and translational disorder are often observed in the assembled NRs. Anisotropic interactions between NRs can be more important for their self-assembly than in the case of NPs,[16] due to their cylindrical geometry and related coupling forces.

NRs with larger aspect ratios $L/D > 2.5$ preferentially self-assemble in *parallel* orientation with respect to the substrate,[12,22,23,25] possibly due to their large coupling to the surfaces. Such NRs have been also prepared in superlattices of *vertically* oriented NRs on electrically conducting substrates,[30,32] where the dipole−substrate coupling might be important.[16] The application of external electric fields[26,28] allows the assembly of vertically oriented CdSe and CdS NRs even with large aspect ratios $L/D \approx 5-6$ when the substrates are potentially less relevant during the self-assembly. Electric field can also reorient nematic alignments of CdSe and CdTe NRs with $L/D < 10$ on the substrate.[29]

NRs with smaller aspect ratios $L/D \approx 1-2.5$ self-assemble into superlattices with a broad range of packing types. Some patterns of horizontal NRs are organized in "tracks",[23] as in the smectic-A (sA) liquid crystal phase.[27] These NRs can also form close-packed simple hexagonal (SH) superlattices of vertically oriented NRs, self-assembled in several layers.[23,24,30,31]

In this work, we theoretically investigate under which conditions semiconducting NRs self-assemble into experimentally observed superlattices. The analysis is done by considering van der Waals (vdW) and Coulombic interactions between the system components, as in the case of monodisperse nanoparticles.[16]

2. Theoretical Modeling. In Figure 1, we schematically show the coordinate system and the coupling terms between individual NRs that are modeled as solid cylinders of the length L and the diameter D. Coupling of NRs with hexagonal cross sections is briefly estimated as well. The total coupling energy between two NRs can be described by the formula

$$V(ij) = V^{\mathrm{vdW}}(ij) + V^{\mathrm{ster}}(ij) + V^{\mathrm{D}}(ij) \quad (1)$$

Here, $V^{\mathrm{vdW}}(ij)$ is the vdW coupling energy between the ith and jth NRs, $V^{\mathrm{ster}}(ij)$ is the energy of their steric repulsion, modeled by the hard-sphere form,[16] and $V^{\mathrm{D}}(ij)$ is their dipole−dipole potential energy.

The van der Waals Coupling. The vdW potential energy $V^{\mathrm{vdW}}(ij)$ in eq 1 can be approximately calculated by the

* Corresponding author: pkral@uic.edu.

10.1021/nl801530x CCC: $40.75
Published on Web 10/14/2008

Table 1. Summary on the Colloidal Nanorod Superlattices

D (nm)	L (nm)	L/D	material	μ (D)	ordering/substrate orientation
3.0−6.5	7.5−40	2−12	CdSe	29−971	nematic/parallel [12]
3.0−3.7	18−60	6−20	CdSe	69−354	nematic/parallel [22]
3−5	10−40	2−10	CdSe−CdS	77−863	nematic and smectic/parallel; SH perpendicular [23]
3−5	4−50	1−10	CdS	76−2650	smectic/parallel[25]
5	30	6	CdS	1590	SH perpendicular (field assisted)[26]
8	40	5	CdSe	1105	SH perpendicular (field assisted)[28]
3.4/6	38/50	11.1/8.4	CdSe/CdTe	189/−	nematic parallel (field assisted)[29]
5.2	24	4.6	CdSe−CdS	560	SH perpendicular[24]
10	25	2.5	CdS	5300	SH perpendicular (HOPG)[30]
5	15	3	CdS	795	SH perpendicular; parallel[31]

Hamaker pairwise summation.[33] In general, it cannot be obtained in analytical form, but we can get it by integrating over coupled volume elements in the formula

$$V^{\mathrm{vdW}}(ij) = -\frac{A}{\pi^2}\int_{V_i}\int_{V_j}\frac{1}{r^6}\,\mathrm{d}\vec{r}_i\,\mathrm{d}\vec{r}_j \tag{2}$$

where ρ is the material density and $A = C\pi^2\rho^2$ denotes the Hamaker constant. Due to the fast $1/r^6$ decay of the vdW coupling, we couple only the nearest NR neighbors.

The NRs are considered in the side-by-side or face-to-face configurations, schematically shown in Figure 1b. If the cylinders are aligned side by side, with a small spacing between them, an analytical expression for the vdW coupling energy can be found from eq 2 in the form[34]

$$V_{\mathrm{RS}}{}^{\mathrm{vdW}}(d) = -\frac{AL\sqrt{R}}{24d^{3/2}} \tag{3}$$

Here, d denotes the nearest distance between the two NRs, assumed to be approximately twice the thickness of the surfactant layer $d/2 \approx 1$ nm. This formula is valid only when $d \ll R$, so it can only be used for the interaction between the nearest NR neighbors considered here. Similarly, we can estimate the vdW coupling between two face-to-face stacked NR cylinders[34]

$$V_{\mathrm{RF}}{}^{\mathrm{vdW}}(d) = -\frac{AR^2}{12}\left(\frac{1}{d^2} - \frac{1}{(d+L)^2} - \frac{2}{(d+2L)^2}\right) \tag{4}$$

This expression also holds only in the case of $d \ll R$, and it is thus applicable for the nearest NRs.

Finally, we also need to evaluate the vdW coupling of the NRs with the substrate from eq 2. We can easily find the expressions

$$V_{\mathrm{SS}}{}^{\mathrm{vdW}}(d_{\mathrm{S}}) = -\frac{A_{\mathrm{S}}LR^2}{6(d_{\mathrm{S}}(2R+d_{\mathrm{S}}))^{3/2}} \tag{5}$$

$$V_{\mathrm{SF}}{}^{\mathrm{vdW}}(d_{\mathrm{S}}) = -\frac{A_{\mathrm{S}}R^2}{12}\left(\frac{1}{d_{\mathrm{S}}{}^2} - \frac{1}{(d_{\mathrm{S}}+L)^2}\right) \tag{6}$$

which are valid for the side-to-substrate and face-to-substrate orientations of the NRs, respectively. Here, A_{S} denotes the effective Hamaker constant for the coupling between the NR and the substrate, separated by the distance d_{S}.

We can also estimate the vdW coupling energy between parallel NRs with hexagonal cross section of the same area as in NRs with circular cross section. In both cases, the minimum distance between neighboring NRs is $d = 2$ nm. The coupling energies are calculated from eq 2, where we integrate over the volumes of neighboring NRs with different cross sections. The hexagonal cross section increases the vdW coupling energy by 17−40% for NRs with diameters of $D = 4$−6 nm, respectively, due to larger side-to-side contact between them.

While the vdW coupling between NRs cores might be relatively weak during the self-assembly process in the solvent, it probably becomes essential after the solvent evaporates due to direct percolation of surfactants from

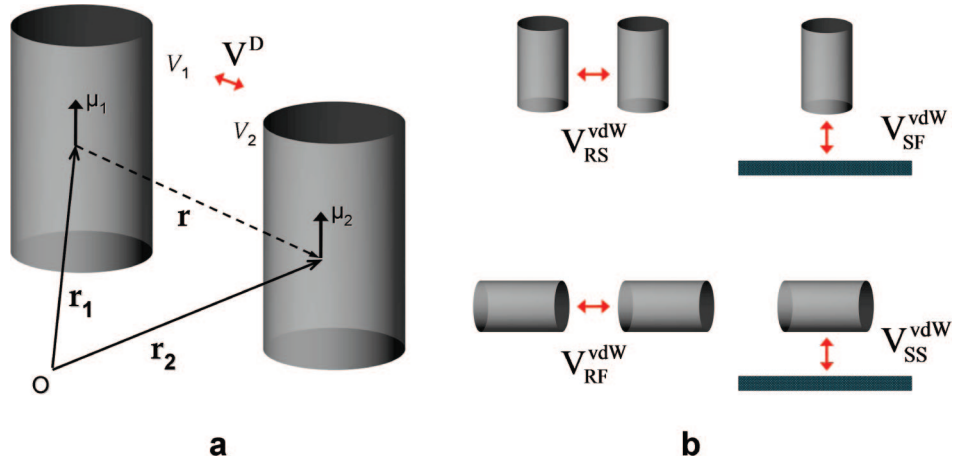

Figure 1. (a) The coordinate system for a pair of cylindrical NRs with a dipolar density μ and interaction potential energy V^{D}. (b) The vdW coupling terms in the self-assembled layers of NRs. The $V_{\mathrm{RS}}{}^{\mathrm{vdW}}$ and $V_{\mathrm{RF}}{}^{\mathrm{vdW}}$ potential energies represent the side-to-side and face to-face interactions between pair of NRs, respectively. The $V_{\mathrm{SS}}{}^{\mathrm{vdW}}$ and $V_{\mathrm{SF}}{}^{\mathrm{vdW}}$ terms stand for the side-to-substrate and face-to-substrate interactions between a NR and the substrate, respectively.

different NRs (NPs).[35−37] In this work, we do not consider this vdW coupling of the surfactants in the absence of solvent.

The Dipole−Dipole Coupling. We estimate first the permanent dipole moments of the semiconducting CdSe NRs. The CdSe lattice has a wurtzite structure with intrinsic polarity,[38−40] due to the lack of inversion symmetry.[41] Therefore, the NR dipoles scale linearly with the rod volume.[42] We can evaluate them from μ (debye) $= \rho_d \mathcal{V}$ (nm^3), where $\rho_d = 0.55$ and 2.7 (D/nm^3) is the dipolar density for the CdSe and CdS crystals, respectively.[41,42] We consider a uniform distribution of point dipoles inside the cylinder of the volume $\mathcal{V} = \pi D^2 L/4$, giving the total dipole moment $\mu = \rho_d \mathcal{V}$.

The dipole−dipole (D−D) coupling term in eq 1 can be obtained by integrating the dipolar distribution over the volumes V_1 and V_2 of both NR cylinders,[43] as shown in Figure 1a,

$$V^D(ij) = \rho_d^2 \int_{V_1}\int_{V_2} \frac{-3(\hat{\mu}_1\cdot\hat{r})(\hat{\mu}_2\cdot\hat{r}) + \hat{\mu}_1\cdot\hat{\mu}_2}{4\pi\varepsilon_0\varepsilon_1 r^3}\, d\vec{r}_i\, d\vec{r}_j \quad (7)$$

Here $\hat{\mu}_i$ and $\hat{\mu}_j$ are the unit vectors directed along the dipoles of cylinders 1 and 2, respectively, $\vec{r}_i$ and $\vec{r}_j$ are the positions of the local dipoles within these cylinders, and $\vec{r} = \vec{r}_i - \vec{r}_j$, $\hat{r} = \vec{r}/r$, where $r = |\vec{r}|$. The effective dielectric constant ε_1 is a combination of dielectric constants for the solvent ($\varepsilon_{toluene} \approx 2.4$) and the surfactants. Since the D−D energies of the self-assembled superlattices can be easily scaled with ε_1, we calculate them for $\varepsilon_1 = 1$.

We cannot obtain a simple analytic expression for a short-range D−D coupling between the NRs, but the interaction potential energy can be calculated numerically and tabulated. If the NR axes are parallel to each other in the superlattice, so their dipoles point up or down, then the $V^D(ij)$ function depends only on their relative radial and axial coordinates. For the considered NR sizes, it can be tabulated like a two-parametric function.

In the limit of large distances ($r_C > 50$ nm) between the NRs, the dipole−dipole (D−D) coupling term in eq 1 can be used in the form[43]

$$V^D(ij) \approx \frac{-3(\vec{\mu}_i\cdot\hat{r}_C)(\vec{\mu}_j\cdot\hat{r}_C) + \vec{\mu}_i\cdot\vec{\mu}_j}{4\pi\varepsilon_0\varepsilon_1 r_C^3} \quad (8)$$

where $\vec{\mu}_i$ and $\vec{\mu}_j$ are the total dipoles of the ith and jth NRs, respectively, and $\hat{r}_C = \vec{r}_C/r_C$ is the unit vector joining the centers of the cylinders.

Polarization of NRs in Electric Fields. The energy of a single polar and polarizable NR in the electric field $\vec{\mathcal{E}}_1$, present in the medium surrounding the NR and oriented along its axis, is given by

$$E^{field} = \vec{\mathcal{E}}_1\cdot\vec{\mu} - \frac{1}{2}\alpha\vec{\mathcal{E}}_1^2 \quad (9)$$

where α is the polarizability of the NR along its axis. The induced dipole $\vec{m}$ of the NR with the volume $\mathcal{V}$ and the polarization $\vec{P}$ is given by

$$\vec{m} \equiv \alpha\vec{\mathcal{E}}_1 = V\vec{P} \quad (10)$$

The polarization $\vec{P}$ can be represented through the internal electric field $\vec{\mathcal{E}}_2$ inside the NR as $\vec{P} = (\varepsilon_2 - 1)\vec{\mathcal{E}}_2/4\pi$. This gives the expression for the induced dipole[44]

$$\vec{m} = \mathcal{V}\,\frac{\varepsilon_2 - 1}{4\pi}\,\frac{\varepsilon_1}{\varepsilon_1 + (\varepsilon_2 - \varepsilon_1)A}\vec{\mathcal{E}}_1 \quad (11)$$

where A is the depolarization factor along the NR axis and ε_1 and ε_2 are the dielectric constant of the outer medium and the NR, respectively.

In the case of a prolate spheroid with the semiaxes a and b, where $a \gg b$, the depolarization factor A can be obtained analytically[45]

$$A = \frac{1}{m^2 - 1}\left[\frac{m}{2(m^2-1)^{1/2}}\ln\left(\frac{m + (m^2-1)^{1/2}}{m - (m^2-1)^{1/2}}\right) - 1\right] \quad (12)$$

where $m = a/b$. For simplicity, we use the above energy contributions from polarized isolated NRs even in the presence of a superlattice, since their value is small.

The Total Energy. After combining all the above terms for the system of N NRs assembled on the substrate, we obtain the total energy per NR in the following form

$$E^{tot} = \frac{1}{N}\sum_{i<j}^{N} V(ij) + V^{surf} + E^{field} \quad (13)$$

$$V^{surf} = V_{surf}^{vdW} + \frac{1}{2}\sum_{i}^{N} V_i^I$$

Here $V(ij)$ values are formed by the pairwise vdW coupling (3) or (4) terms, as well as by the D−D coupling (7) and (8). The V^{surf} potential energy is formed by the vdW coupling (5) or (6) and Coulombic coupling to the electrically conducting substrate. The last coupling is realized through image charges,[16] where V_i^I is the coupling energy between the dipoles of the ith NR with all the mirrored dipoles.[46] The last term in eq 13 accounts for the coupling of the NRs to the electric field in the medium, given by eq 9. When we calculate the total energies of different NR superlattices from eq 13, we keep the NRs at fixed separations of $d = 2$ nm. The obtained results are used to identify the stable structures with the lowest total energy.

3. Results and Discussion. 3.1. Characteristic Interactions between NRs. We first estimate the coupling terms in pairs of typical CdSe NRs[12,22,23,25] of the diameter $D = 6$ nm and ratios of $L/D = 8.3$ and 2.0. These NRs possess the dipole of $\mu = \rho_d \mathcal{V} \sim 778$ and 187 D, respectively. The dielectric constant along the symmetry axis of the CdSe lattice[42] is $\varepsilon_2 = 10.2$. We also model the effective dielectric constant of the medium by $\varepsilon_1 = 1$. The NRs are face-to-face or side-by-side separated by $d = 2$ nm. Their face-to-substrate and side-to-substrate distance is $d_S \approx 1$ nm, since only the NRs are passivated with capping ligands. The Hamaker constant for the CdSe/hexane/CdSe vdW coupling is $A \approx 0.3$ eV.[47] The Hamaker constant for the vdW coupling to the amorphous carbon substrate is $A_S \approx 0.4$ eV for CdSe NR (0.34 eV for CdS NR).[47,48]

From eqs 3, 4, and 7, we calculate the NR−NR and NR−substrate coupling energies for the two L/D ratios and present the results in Table 2. For the larger L/D ratio, the

Table 2. Characteristic coupling terms for the CdSe NRs with two different size ratios. The energies are given in eV.

L/D	V_{RS}^{vdW}	V_{RF}^{vdW}	V_{SS}^{vdW}	V_{SF}^{vdW}	V_{RS}^{D}	V_{RF}^{D}	V_{S}^{I}	V_{F}^{I}
8.3	−0.382	−0.56	**−1.62**	−0.3	−0.034	−0.041	−0.017	−0.020
2.0	−0.092	−0.054	−0.389	−0.298	−0.019	−0.032	−0.009	−0.016

side-to-substrate vdW coupling V_{SS}^{vdW} dominates. This explains why long NRs aggregate into close-packed nematic and smectic phases horizontally oriented on substrates (Table 1).[12,22,23] For the smaller L/D ratio, the V_{SS}^{vdW} and V_{SF}^{vdW} couplings are comparable, and the face-to-substrate coupling eventually dominates. The D−D coupling is calculated in the *antiferroelectric* (A) ordering of dipoles in vertically arranged NRs (SH-A) and in the "aligned" ordering of dipoles for horizontally arranged NRs (sA-A).[16] The vdW and D−D couplings between NRs are relatively small, but in the presence of many NRs (several neighbors) they can significantly contribute to the competition between the horizontal or vertical arrangement of the NRs on the substrate.

3.2. Stable Phases of Many NRs. The vertical stacking of NRs on substrates should be possible to stabilize by the discussed vdW and Coulombic coupling. Since the D−D coupling might be small, we separately model the NR stabilization by the vdW coupling. We can easily find that a *single* NR is stable on the substrate in the vertical orientation if its face-to-substrate vdW coupling, $V_{SF}^{vdW}(d_S)$, is stronger than its side-to-substrate vdW coupling, $V_{SS}^{vdW}(d_S)$. For $d_S = 1$ nm and $4 < D < 11$ nm, these coupling energies are approximately the same if $L \approx 1.75D$; i.e., the vertical orientation is more stable for $L < 1.75D$. The aspect ratio of $L/D = 1.75$ roughly agrees with the experimentally obtained data for NRs self-assembled in the vertical stacking[24,30,49] (Table 1).

Let us consider the vdW coupling between many NRs. In a monolayer superlattice, each NR in a SH-phase has six contacts with its nearest neighbors and one contact with the substrate, so the energy per NR is

$$E_{SH}^{vdW} = 3V_{RS}^{vdW} + V_{SF}^{vdW} \quad (14)$$

Similarly, in the sA-phase the NR has two side and two face neighbors, so the coupling energy per NR is

$$E_{sA}^{vdW} = V_{RS}^{vdW} + V_{RF}^{vdW} + V_{SS}^{vdW} \quad (15)$$

If the monolayer or a multilayer slab forms a cluster, the NRs at the peripheral or upper/lower boundaries have frustrated coupling to fewer neighbors. This gives fewer coupling terms and results in an effective "boundary" energy, which is analogous to the surface energy used in molecular clusters. On a straight periphery of a monolayer, each NR has two fewer neighbors in the SH-phase and one fewer (face or side) neighbor in the sA-phase. The missing coupling to these NRs generates the boundary energy of the NR cluster. Analogous contributions come from the vertical direction.

We use eqs 14 and 15 to model the stability of NR phases assembled on a conducting substrate. In Figure 2, we show a phase diagram for the sA and SH phases formed in monolayer clusters with hexagonal symmetries on the conducting substrate. The upper curve is calculated only for

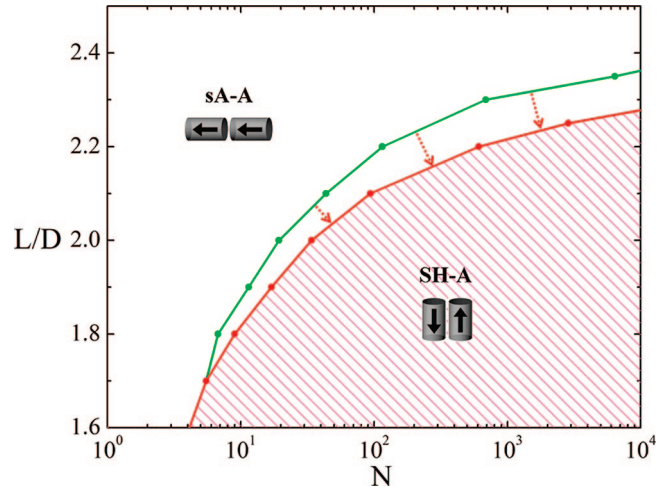

Figure 2. Phase diagram for monolayer clusters with N NRs in the sA and SH phases. The upper curve separates these two phases when only the vdW interactions are considered. The lower curve separates the same phases with antiferroelectric ordering of their dipoles when the Coulombic interactions are also included.

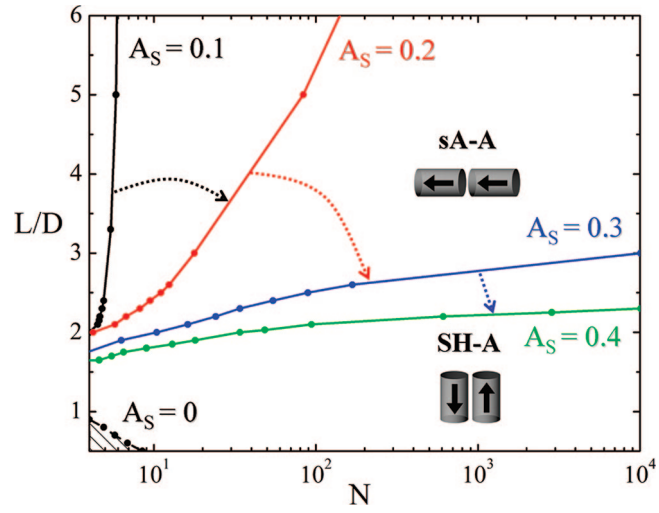

Figure 3. Phase diagram of a monolayer with N NRs of different sizes at different vdW coupling with the substrate, described by the Hamaker constant A_S. The region with the SH-A packing becomes larger when A_S is smaller. A small region of sA-A discotic-like packing emerges as $A_S \to 0$. The SH-A superlattice observed experimentally at ratio $L/D = 4.6$ agrees with our phase diagram at smaller vdW coupling ($A_S \approx 0.2$).[24] The same is true for the experiments with vertically assembled NRs with the ratio $L/D = 2.5$.[30]

the vdW coupling, where $A_S \approx 0.4$ eV as before. In the regions shown, the two phases have lower total energies, while entropic effects are neglected in this zero-temperature study.[16] We find the phase boundary for different L/D ratios by varying the cylinder length L, but keeping the NR diameter fixed at $D = 6$ nm. The results are shown for different numbers of NRs, N, in order to describe the effect of boundary energies on the stability of these clusters. We can see that the vertical orientation of NRs is achieved in large NR domains with $L/D \approx 1.6-2.3$. These results modify the above single-NR solution with $L/D = 1.75$.

We now switch on also the D−D coupling between pairs of NRs and their Coulombic coupling to the dipole images

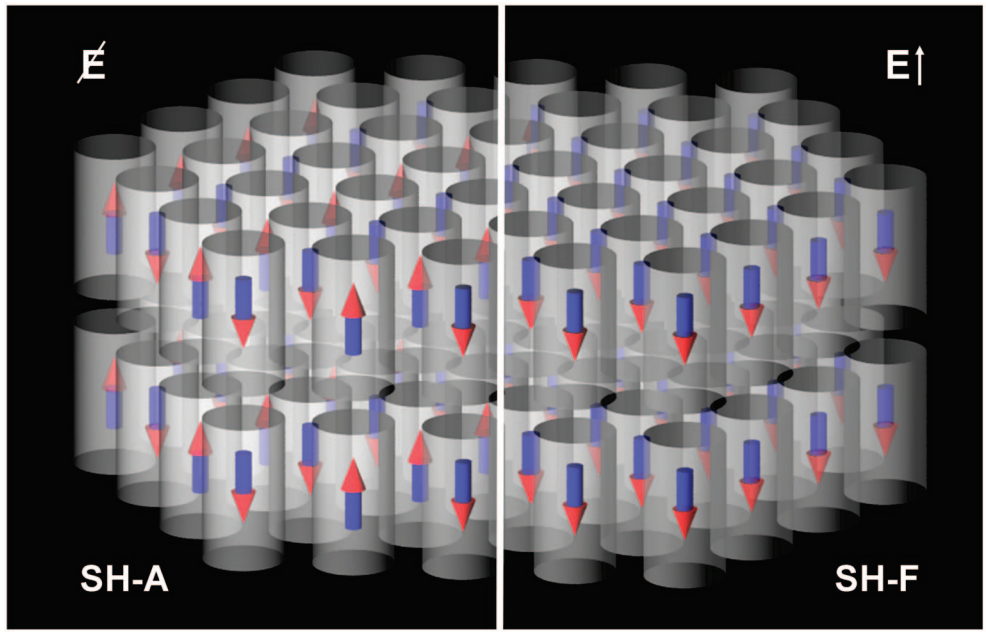

Figure 4. (left) Nanorods in the SH-A bilayer cluster with a hexagonal symmetry formed on the substrate. The NR dipoles are vertically oriented in the antiferroelectric order, which provides the lowest possible energy. (right) Nanorods in a bilayer SH−F cluster with a hexagonal symmetry that are formed perpendicularly to the substrate in the presence of electric field. The NR dipoles are oriented in the ferroelectric order antiparallel to the field.

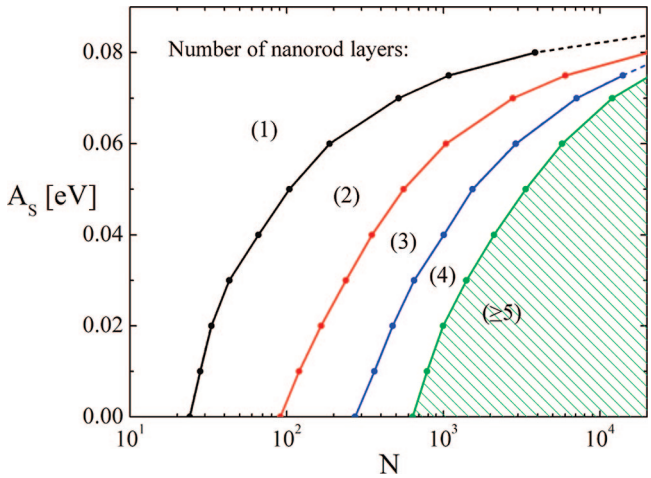

Figure 5. Phase diagram of multilayer SH-A hexagonal cluster. (1), (2), (3), (4), and (≥5) denote the regions of one, two, three, four, and five (and more) stacked layers, respectively.

in the substrate. From Table 2, we can see that the D−D coupling slightly preferentiates the face-to-face over side-to-side coupling of the NRs. As shown in Figure 2 (lower curve), this fact tends to enlarge the antiferroelectric sA-A phase, with the larger head-to-tail connectivity (face-to-face coupling) of the NRs than the SH-A phase. If we use a more realistic effective dielectric constant of $\varepsilon_1 \approx 2-3$, rather than $\varepsilon_1 = 1$ that is considered here, the D−D coupling becomes less relevant and the solution is closer to the case of pure vdW attraction. These results agree well with the experimental data in Table 1, where the SH phase was observed for $L/D \approx 2.5$.[24,30] The phase boundary also roughly agrees with ref 31, where NRs with $L/D \approx 3$ manifest such transition when their concentration is increased. The phase boundaries can be easily extrapolated to larger numbers of NRs.

Let us now see what happens if we decrease the vdW coupling of NRs to the substrate, but keep the other coupling terms (including D−D coupling) as in Figure 2, and assume that the NRs remain in a monolayer. In Figure 3 (left), we can see that as the vdW coupling A_S to the surface is decreased, the region with the SH-A packing becomes larger. This is because the particles become gradually released from the surface and stand up, due to dominant side-to-side vdW coupling between them. When $A_S \rightarrow 0$, the sA-A phase will completely disappear at $L/D > 2$, but it will emerge at $L/D < 0.9$ in a form of discotic-like sA-A phase.

We now also allow the NRs to form multilayer clusters, while their vdW coupling A_S to the surface is decreased. The clusters formed are displayed for bilayers in Figure 4 (left). As in Figure 3, we start from a SH-A monolayer of CdSe NRs, but we fix $L/D = 2$ ($D = 6$ nm) and allow the formation of multilayers. Again, the clusters with certain number N of NRs are gradually released from the substrate by weakening their vdW coupling (A_S) to it. But now the boundary energy can play a role in stabilization of clusters with different numbers of layers, for the same number N of NRs. The formation of multilayer NR clusters is governed by similar rules as the formation of droplets on partially wetting surfaces.

In Figure 5, we show the phase diagram for the stable SH-A clusters with different number of layers with hexagonal symmetries. The results are calculated from eq 13 and presented as a function of the Hamaker constant A_S, for the NR−substrate coupling, and the number N of NRs. At larger A_S (much smaller than in Figure 2) and smaller N the most stable arrangement is a monolayer of NRs tightly packed in a cluster with a hexagonal shape. When A_S becomes smaller or N larger, a twice smaller hexagonal cluster with NRs in

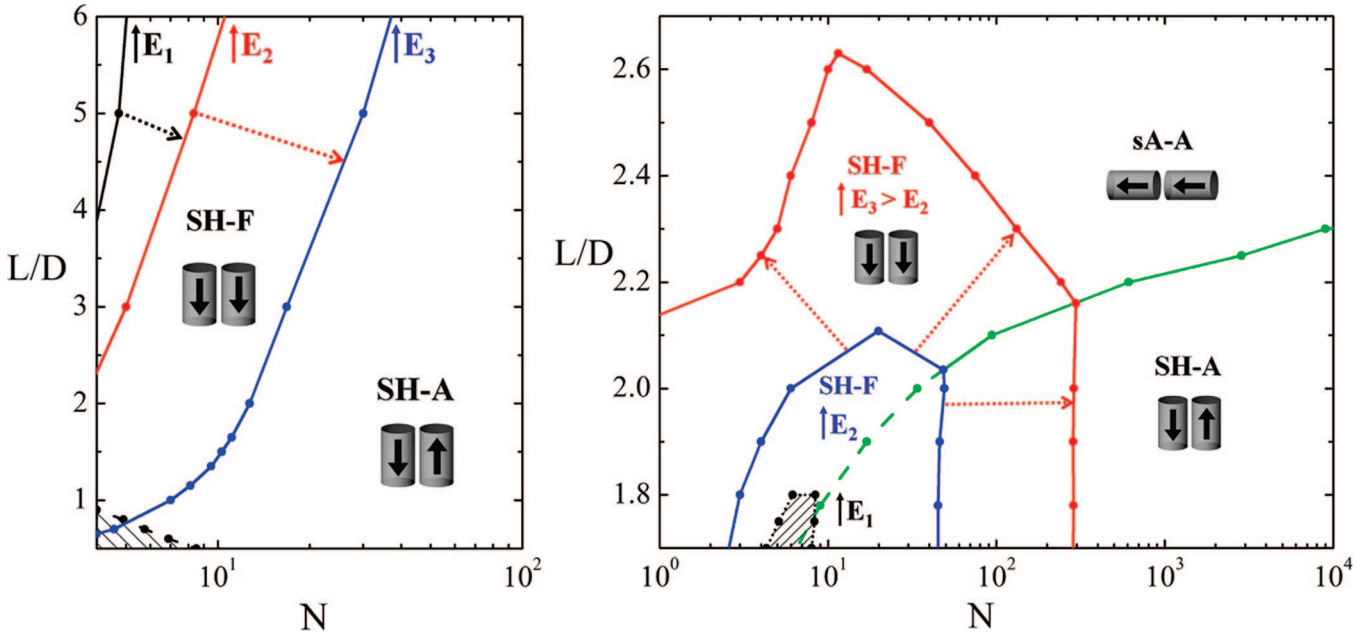

Figure 6. (left) The transition between SH-A and SH-F packing in a monolayer and in the presence of vertically oriented electric fields $\mathcal{E}_1 = 1$ V/μm, $\mathcal{E}_2 = 5$ V/μm, and $\mathcal{E}_3 = 10$ V/μm. The vdW coupling to the substrate is absent ($A_S = 0$). The SH-F phase with ferroelectric order spreads more at larger fields. At the ratio of $L/D = 5$, 6, we observe vertical orientation of NRs at small fields, which is in agreement with refs 26 and 28 as shown in Table 1. (right) Phase diagram of a monolayer with N NRs of different sizes in the presence of stronger electric fields. Without fields, the transition between superlattices with the sA-A and SH-A packing is controlled by the material parameters (Figure 2). In the presence of the electric fields, $\mathcal{E}_1 = 10$ V/μm, $\mathcal{E}_2 = 20$ V/μm, and $\mathcal{E}_3 = 30$ V/μm, a new SH phase emerges with NRs oriented in a ferroelectric order (SH-F).

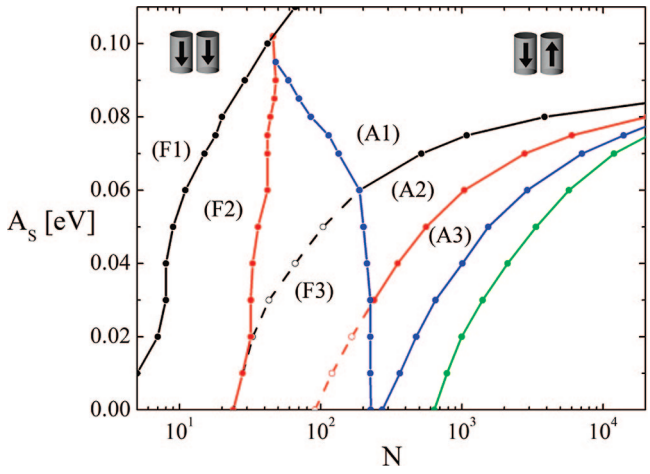

Figure 7. Phase diagram of SH superlattice clusters with N NRs in the electric field of $\mathcal{E} = 20$ V/μm. (F1), (F2), and (F3) denote the regions with ferroelectric ordering of dipoles in one, two, and three layers, respectively. (A1), (A2), and (A3) denote the regions with antiferroelectric ordering of dipoles in one, two, and three layers, respectively.

two layers is eventually formed and later substituted by three layers, and so on. In this "piling" process, the interlayer NR coupling compensates the loss of NR binding energy to the substrate. This is why the piling cannot happen at larger A_S, since the substrate would bind the NRs more than the NRs bind face-to-face one to another. The dependence on N reflects the fact that the monolayer cluster must be broken in two, so the side-to-side binding for some NRs is also lost (the multilayer is again arranged into hexagonal form). Analogous piling of NRs into multilayer SH cluster was observed experimentally[23] when small amounts of hexadecyamines were added to the system. Its aggregation on the substrate might effectively impede the vdW NR−substrate coupling and favor stabilization of the vertical NR superlattices.[23,24] Note that the large vdW coupling between the NR faces prohibits spontaneous self-assembly of HCP and FCC structures, known to form in nanoparticle superlattices.[16]

3.3. Field-Assisted Self-Assembly of NRs. The vertical stacking of NRs could be also stabilized by the Coulombic coupling of the polar and polarizable NRs to electric fields. Recently, superlattices with vertically oriented CdS/CdSe NRs were prepared in the presence of homogeneous electric fields perpendicular to the substrate.[26,28] The superlattices remain preserved when the field is turned off, which might be due to the side-by-side vdW coupling between the NRs and interdigitation of their surfactants upon solvent removal.

We consider first a single (not polarizable) CdS NR, with $L = 30$ nm and $D = 5$ nm, solvated in toluene.[26] We calculate the change of its energy when it rotates from the orthogonal to the parallel orientation with respect to the field of $\mathcal{E} = 1$ V/μm. The energy change is $\Delta U = -p\mathcal{E}/\varepsilon_1 = 13.8$ meV, where $p \approx 1590$ D is the dipole moment of this NR and $\varepsilon_1 = 2.4$ is the dielectric constant of toluene.[50] Since the NR rotation energy ΔU is of the order of the thermal energy $kT \approx 25$ meV, this field should be able to reorient these NRs.

We need to ask whether many NRs can be oriented by the electric field, and if so then what is the structure of the vertically self-assembled NRs. We study the experimentally relevant case of weak electric fields ($\mathcal{E} < 10$ V/μm) and assume that the vdW coupling to the surface is negligible, $A_S = 0$. As before, we include all the coupling terms and

find the equilibrium phases, while neglecting the crystallization kinetics. We calculate the phase diagram for a monolayer cluster of many NRs. As shown in Figure 6 (left), in the absence of the fields the sA-A phase is stable only for the small portion of discotic NRs ($L/D < 0.9$), while the SH-A phase is stable in the rest of the diagram. At the field of $\mathcal{E}_1 = 1$ V/μm, the SH-F phase of ferroelectrically (F) aligned NRs is stable for $L/D > 4$, and at larger fields it becomes stable even for shorter NRs. The SH-A phase remains stable in clusters with more NRs N, since the long-range D−D repulsion in the SH-F phase is too big. The increase in dielectric constant of the medium to $\varepsilon_1 = 2$ shifts the phase boundaries to the right, stabilizing thus the SH-F phase. Here, only the presence of ε_1 in the D−D term is relevant, since the polarization contribution (≈6% of the total energy at $\mathcal{E} = 5$ V/μm) in eq 8 is the same for both types of vertical lattices.

We also address the field-induced reorientation of (shorter nonpolarizable) NRs with $1.7 < L/D < 2.7$ adsorbed in a monolayer cluster on a conducting substrate with $A_S = 0.4$. In Figure 6 (right), we show the phase diagram in the presence of electric field, which is an extension of Figure 2, where a new SH-F phase appears for NRs with a *ferroelectric* vertical dipole ordering. In order to reorient (align) all the NR dipoles along the field direction, the field needs to be here strong enough to overcome not only the repulsive D−D coupling but also the vdW attraction to the substrate. Longer NRs, lying on the substrate in the sA-A phase, are harder to reorient vertically in the SH-F phase, because of their larger vdW and Coulombic coupling to the substrate. Nevertheless, by increasing the electric field from $\mathcal{E}_1 = 10$ V/μm to $\mathcal{E}_2 = 20$ V/μm and $\mathcal{E}_3 = 30$ V/μm, the stability region of the SH-F phase can be extended. In the SH-F lattice the equilibrium distance of the NRs might be also slightly modified by their Coulombic repulsion, but this is neglected here. At $\mathcal{E} = 20$ V/μm the polarization term in eq 9 contributes 27% of the total energy. We do not use the polarization in the diagram, since the energy contributions are about the same for the field oriented in perpendicular or parallel directions to the NR axis. This is due to the fact that the L/D (aspect) ratio is close to 1. Therefore, the stability regions of different phases would not be affected for these L/D ratios.

We also study the formation of multilayer clusters in electric fields for the CdSe NRs with $L/D = 2$ ($D = 6$ nm). The NRs have SH antiferroelectric (A) and ferroelectric (F) ordering of dipoles, shown in Figure 4, respectively. In Figure 7, we present the calculated regions of stability at the field of $\mathcal{E} = 20$ V/μm, which extend the results from the Figure 5. In the presence of the field, the SH-F stacking can be energetically lower than the SH-A stacking, since the D−D repulsion in the former is overcome by the dipole−field coupling. As in the monolayer (Figure 6), the SH-F stacking is more stable for smaller clusters, while the SH-A stacking is stable for larger clusters. The SH-F clusters with two and three layers are stable in narrow regions of N, due to large D−D repulsion, which is not compensated by the dipole−field coupling. At larger A_S and N, the SH-A superlattice is more stable, as seen in Figure 7. Other NR lattices might be stabilized in the presence of electric fields[26] if NR polarization is also considered and the inhomogeneous field formed around NRs is described.

Note that NRs rather easily form SH superlattices, while the assemblies of monodisperse NPs typically form face-centered cubic or hexagonal close packed lattices. This is because NRs have large vdW coupling energies between their flat sides, while in NPs these forces depend practically only on the NP distances. In NP superlattices, the D−D coupling and Coulombic coupling to substrates can establish stable SH lattices only in a rather limited range of parameters.[16]

4. Conclusions. We have modeled the self-assembly of semiconducting NRs interacting mutually and with electrically conducting substrates by van der Waals and Coulombic coupling. The theoretical studies predict phase transitions between clusters of NRs with different lattice types. The results indicate that the aspect ratio L/D and the number of NRs are the most important factors that determine the type of the packing. These phase transitions can be efficiently controlled by external electric fields. The obtained results are in good agreement with the experimentally observed data. This should allow wider applications of the described models in the prediction of potential superlattices that could be self-assembled.

Acknowledgment. We thank Professor Dmitri Talapin and Dr. Elena Shevchenko for many helpful suggestions and discussions.

References

(1) Huynh, W. U.; Dittmer, J. J.; Alivisatos, A. P. *Science* **2002**, *295*, 2425–2427.
(2) Coe, S.; Woo, W. K.; Bawendi, M.; Bulovic, V. *Nature* **2002**, *420*, 800–803.
(3) Gao, X. H.; Cui, Y. Y.; Levenson, R. M.; Chung, L. W. K.; Nie, S. M. *Nat. Biotechnol.* **2004**, *22*, 969–976.
(4) Urban, J. J.; Talapin, D. V.; Shevchenko, E. V.; Kagan, C. R.; Murray, C. B. *Nat. Mater.* **2007**, *6*, 115–121.
(5) Becker, K.; Lupton, J. M.; Muller, J.; Rogach, A. L.; Talapin, D. V.; Weller, H.; Feldmann, J. *Nat. Mater.* **2006**, *5*, 777–781.
(6) Murray, C. B.; Norris, D. J.; Bawendi, M. G. *J. Am. Chem. Soc.* **1993**, *115*, 8706–8715.
(7) Peng, X. G.; Wickham, J.; Alivisatos, A. P. *J. Am. Chem. Soc.* **1998**, *120*, 5343–5344.
(8) Peng, X. G.; Manna, L.; Yang, W. D.; Wickham, J.; Scher, E.; Kadavanich, A.; Alivisatos, A. P. *Nature* **2000**, *404*, 59–61.
(9) Kim, F.; Song, J. H.; Yang, P. D. *J. Am. Chem. Soc.* **2002**, *124*, 14316–14317.
(10) Peng, X. G. *Adv. Mater.* **2003**, *15*, 459–463.
(11) Murray, C. B.; Kagan, C. R.; Bawendi, M. G. *Annu. Rev. Mater. Sci.* **2000**, *30*, 545–610.
(12) Li, L. S.; Hu, J. T.; Yang, W. D.; Alivisatos, A. P. *Nano Lett.* **2001**, *1*, 349–351.
(13) Ahmadi, T. S.; Wang, Z. L.; Green, T. C.; Henglein, A.; ElSayed, M. A. *Science* **1996**, *272*, 1924–1926.
(14) Yu, Y. Y.; Chang, S. S.; Lee, C. L.; Wang, C. R. C. *J. Phys. Chem. B* **1997**, *101*, 6661–6664.
(15) Shevchenko, E. V.; Talapin, D. V.; Kotov, N. A.; O'Brien, S.; Murray, C. B. *Nature* **2006**, *439*, 55–59.
(16) Talapin, D. V.; Shevchenko, E. V.; Murray, C. B.; Titov, A. V.; Král, P. *Nano Lett.* **2007**, *7*, 1213–1219.
(17) Sun, S. H.; Murray, C. B.; Weller, D.; Folks, L.; Moser, A. *Science* **2000**, *287*, 1989–1992.
(18) Huynh, W. U.; Peng, X. G.; Alivisatos, A. P. *Adv. Mater.* **1999**, *11*, 923.
(19) Sun, B. Q.; Marx, E.; Greenham, N. C. *Nano Lett.* **2003**, *3*, 961–963.
(20) Bruchez, M.; Moronne, M.; Gin, P.; Weiss, S.; Alivisatos, A. P. *Science* **1998**, *281*, 2013–2016.

(21) Chan, W. C. W.; Nie, S. M. *Science* **1998**, *281*, 2016–2018.
(22) Li, L. S.; Alivisatos, A. P. *Adv. Mater.* **2003**, *15*, 408–411.
(23) Talapin, D. V.; Shevchenko, E. V.; Murray, C. B.; Kornowski, A.; Forster, S.; Weller, H. *J. Am. Chem. Soc.* **2004**, *126*, 12984–12988.
(24) Talapin, D.; Nelson, J.; Shevchenko, E.; Aloni, S.; Sadtler, B.; Alivisatos, A. *Nano Lett.* **2007**, *7*, 2951–2959.
(25) Ghezelbash, A.; Koo, B.; Korgel, B. A. *Nano Lett.* **2006**, *6*, 1832–1836.
(26) Ryan, K. M.; Mastroianni, A.; Stancil, K. A.; Liu, H. T.; Alivisatos, A. P. *Nano Lett.* **2006**, *6*, 1479–1482.
(27) de Gennes, P.; Prost, J., *The physics of liquid crystals*; Clarendon Press: Oxford, 1993.
(28) Gupta, S.; Zhang, Q. L.; Emrick, T.; Russell, T. P. *Nano Lett.* **2006**, *6*, 2066–2069.
(29) Hu, Z. H.; Fischbein, M. D.; Querner, C.; Drndic, M. *Nano Lett.* **2006**, *6*, 2585–2591.
(30) Ahmed, S.; Ryan, K. M. *Nano Lett.* **2007**, *7*, 2480–2485.
(31) Kang, C.-C.; Lai, C.-W.; Peng, H.-C.; Shyue, J.-J.; Chou, P.-T. *ACS Nano* **2008**, *2*, 750–756.
(32) Chen, X. D.; Hirtz, M.; Rogach, A. L.; Talapin, D. V.; Fuchs, H.; Chi, L. F. *Nano Lett.* **2007**, *7*, 3483–3488.
(33) Hamaker, H. C. *Physica* **1937**, *4*, 1058–1072.
(34) Erbil, H. Y., *Surface Chemistry of Solid and Liquid Interfaces*; Blackwell Publishing: Oxford, 2006.
(35) Chen, Z. Y.; Moore, J.; Radtke, G.; Sirringhaus, H.; O'Brien, S. *J. Am. Chem. Soc.* **2007**, *129*, 15702–15709.
(36) Chen, Z.; O'Brien, S. *ACS Nano* **2008**, *2*, 1219–1229.
(37) Vukovic, L., Titov, A., and Král, P. Unpublished.
(38) Blanton, S. A.; Leheny, R. L.; Hines, M. A.; Guyot-Sionnest, P. *Phys. Rev. Lett.* **1997**, *79*, 865–868.
(39) Huong, N. Q.; Birman, J. L. *J. Chem. Phys.* **1998**, *108*, 1769–1772.
(40) Rabani, E.; Hetenyi, B.; Berne, B. J.; Brus, L. E. *J. Chem. Phys.* **1999**, *110*, 5355–5369.
(41) Nann, T.; Schneider, J. *Chem. Phys. Lett.* **2004**, *384*, 150–152.
(42) Li, L. S.; Alivisatos, A. P. *Phys. Rev. Lett.* **2003**, *90*, 097402.
(43) Jackson, J. *Classical electrodynamics*, 2nd ed.; John Wiley & Sons: New York, 1962.
(44) Böttcher, C. J. F. *Theory of electric polarization*; Elsevier: Amsterdam, 1973.
(45) Osborn, J. A. *Phys. Rev.* **1945**, *67*, 351–357.
(46) Diaz, R. A.; Herrera, W. J.; Nino, J. V. *Eur. J. Phys.* **2006**, *27*, 1391–1398.
(47) Ge, G. L.; Brus, L. *J. Phys. Chem. B* **2000**, *104*, 9573–9575.
(48) Li, J. L.; Chun, J.; Wingreen, N. S.; Car, R.; Aksay, I. A.; Saville, D. A. *Phys. Rev. B* **2005**, *71*, 235412.
(49) Saunders, A. E.; Ghezelbash, A.; Smilgies, D. M.; Sigman, M. B.; Korgel, B. A. *Nano Lett.* **2006**, *6*, 2959–2963.
(50) Ruoff, R. S.; Tse, D. S.; Malhotra, R.; Lorents, D. C. *J. Phys. Chem.* **1993**, *97*, 3379–3383.

NL801530X